Electrochemical Production of ZnO and ZnO@Ag Core-Shell Nanorods on ITO Substrate and Their Photocatalytic and Photoelectrochemical Performance

Handan Kamış, Nadiye Duyar Karakuş, Bircan Haspulat Taymaz[1]*

Abstract: Zinc oxide (ZnO) and Ag deposited ZnO (ZnO@Ag) core-shell nanorods produced electrochemically on indium tin oxide coated glass (ITO) substrate for the first time without any organic surfactants or high annealing temperature. Nanorod films were synthesized two-step synthesis procedure. Firstly, ZnO nanorods electrodeposited at low temperature, in second step, in situ electrochemically etching of deposited ZnO nanorod was carried out. Characterizations of electrochemically produced films have been carried by using morphologic, spectroscopic and structural analysis methods by using X-ray diffraction (XRD), scanning electron microscope (SEM), atomic force microscope (AFM), fourier transform infrared spectroscopy (FTIR), Elemental mapping, UV-visible diffuse absorption spectra and photoluminesance spectroscopy (PL). The photocatalytic performance of the obtained films was determined by degradation of methylene blue and malachite green dyes under UV light illumination. Methylene blue and malachite green dyes completely degraded under UV light irradiation after 150 and 180 min, respectively. Also, photoelectrochemical (PEC; water splitting) performances of the produced films were investigated under dark conditions and UV light irradiation. The ZnO@Ag core-shell nanorods exhibited higher photocatalytic and photoelectrochemical performance in comparison with unmodified ZnO nanorods film. The nanorods grown on the ITO substrates showed very good photocatalytic activity and became reusable without significant loss of activity.

Keywords: Electrodeposition, core-shell nanorods, ZnO, photocatalysis, photoelectrochemical.

1. Introduction

chemicals produced by industrial processes are discharged into the environment on a daily basis. As the use of synthetic dyes increases, paint removal becomes an important but challenging area of research in wastewater treatment, since most dyes and their degradation products may be carcinogenic and toxic to mammals (Udom et al. 2013). Therefore, decolorization and detoxification of dye-containing wastewater need to be conducted before discharging wastewater into natural water. Certain physical, chemical, and biological treatments are currently being used for dye wastewater treatment. Although, the complete degradation of the dyes is not possible by conventional methods such as precipitation, adsorption, flocculation, flotation, oxidation, reduction, electrochemical, aerobic, anaerobic, and biological treatment methods. Recently, heterogeneous photocatalysis has emerged as a major degradation technology that leads to total mineralization of organic pollutants, especially synthetic dyes. There are a number of semiconductor metal oxides, such as TiO2, ZnO, SnO, NiO, Cu2O, Fe3O4, and WO3, that could be used as photocatalysts due to their nontoxic nature, high photosensitivity, wide band gap and high stability (Skompska and Zarebska 2014; Udom et al. 2013). ZnO is one of the most

Konya Technical University, Department of Chemical Engineering, Konya, Turkey
*Corresponding author (İletişim yazarı) bhaspulat@ktun.edu.tr

noticeable metal oxide semiconductors. The excellent properties of the material are produced by oxygen vacancy and zinc intervals. ZnO is also biocompatible, biodegradable and includes biosecurity for medical and environmental applications (Fabbri et al. 2016).

Up to now, in most photocatalytic work, sludge-like mixtures of semiconductor material particles and paint solution were used; these were difficult to remove from the treated water. Alternatively, the photocatalyst may be grown or immobilized on a suitable solid inert support which removes the need for photocatalyst removal. Due to their good the photocatalytic and photoelectrochemical properties, the highly porous and nanocrystalline semiconductor thin films are remarkable in recent years. The high surface area also provides more adsorbing area for film contaminants. The ZnO nanostructures/films have been used in different application areas such as, Sensor (Fabbri et al. 2016; Öztürk et al. 2016; Yoo et al. 2015; Vanalakar et al. 2015), UV Detector (Shewale and Yu 2016), UV Laser (Wang and Su 2016), Light-Emitting Diode (Wang and Su 2016), Dye-Sensitized Solar Cells (Rahman et al. 2015), Field Effect Transistor (Zulkifli, Kalita, Tanemura 2015), Photoelectrochemical application (Ge et al. 2015), Electrocatalysis (Li et al 2015), Photocatalysis (Bechambi et al. 2015; Bu 2015; Kaneva, Dimitrov, and Dushkin 2011; Khataee et al. 2015; Li et al 2015; Xu et al. 2012; Zhang et al. 2012) due to the unique electrical, optical, and mechanical properties. Although ZnO has a wide range of application areas, its photocatalytic performance is has drawn much attention for wastewater treatment and clean energy production.

ZnO films has been grown by using various synthesis methods, such as a chemical vapor deposition (Ge et al. 2015; Wang and Su 2016), chemical bath deposition (Wang and Su 2016), pulsed laser deposition (Kang et al. 2006; Shewale and Yu 2016), sol–gel route (Bu 2015; Fabbri et al. 2016; Kaneva, Dimitrov, and Dushkin 2011; Li et al 2015a; Tang et al. 2015), hydrothermal synthesis (Bechambi et al. 2015; Ge et al. 2015; Rahman et al. 2015; Yoo et al. 2015), wet chemical method (Vanalakar et al. 2015), spray pyrolysis technique (Amiri et al. 2016), metal organic chemical vapor deposition (Chikoidze et al. 2008; Habibi and Shojaee 2015; Nam, Kim, and Leem 2015), sole gel spin-coating method (Habibi and Shojaee 2015), chemical

vapor deposition (Li et al 2015a), electrochemical deposition techniques (Chen et al. 2013; Kim, Moon, and Lee 2012; Li et al. 2015b; Orhan and Baykul 2012; Öztürk et al. 2016; Xu et al. 2012). The electrochemical deposition has been accepted as an effective method for preparing nanomaterials because it is a simple, economical, non-vacuuming and low temperature process and can be easily scaled to industrial level.

Several groups have investigated the production of ZnO films by electrochemical deposition method. Öztürk et al (Öztürk et al. 2016) synthesized ZnO nanorods on the quartz crystal microbalance for volatile organic compound sensors by using galvanostatic deposition method and they have annealed the ZnO thin film at 200°C. A ZnO thin film has been prepared by a potentiostatic deposition method on Zn/Si substrates and the produced materials were calcined at 300°C (Kim, Moon, and Lee 2012). Grafted oxide-ZnO nanocomposite films were fabricated by electrochemical deposition on a Fluorine doped Tin Oxide coated glass substrate. Nanocomposite films were produced in three stages: preparation of suspensions, electrochemical deposition of composites and heat treatment while using monoethanolamine as a stabilizer (Li et al. 2015b). ZnO nanorods were grown on indium-tin oxide (ITO) coated glass substrates in two steps consisting of the galvanostatic and the potentiostatic process, and morphological, structural and optical properties of synthesized films were investigated (Orhan and Baykul 2012). ZnO film was electrodeposited potentiostatically on ITO substrate potentiostatically and calcined in air at 400 °C. ZnO films with different modifications of Au and Ag have been investigated to investigate the morphology, optical properties and effect of photocatalytic activity of Ag and Au nanoparticles (Chen et al. 2013).

The electrical and optical properties of ZnO nanostructures can be easily changed to controlled with controlled size, morphology and doping level. ZnO nanomaterial metal doping includes Mg (Shewale and Yu 2016), In (Nam, Kim, and Leem 2015; Tang et al. 2015), Ce Li et al 2015a, Pd (Öztürk et al. 2016), Eu (Chandrasekhar et al. 2015; Khataee et al. 2015), Co (Habibi and Shojaee 2015), Er (Bu 2015), Al (Bu 2015; Yoo et al. 2015), Ni (Kaneva, Dimitrov, and Dushkin 2011), Cu (Li et al 2015a; Wang and Su 2016), Fe (Amiri et al. 2016), Ag (Ansari et al. 2014; Braiek

et al. 2015; Hsu et al. 2014; Kumari et al. 2015; Mosquera et al. 2015; Patil et al. 2016; Sahu et al. 2012) and nonmetal doping includes F (Li et al 2015a), C (Ge et al. 2015; Li et al. 2015b), N (Bu 2015), and Cl (Chikoidze et al. 2008). To produce p-type conductivity and enhance luminescence yield of ZnO doped with silver where its acts as an electron acceptor in the material (Bechambi et al. 2015; Kang et al. 2006). Also, it has been showed that the photocatalytic and photoelectrochemical activity of the ZnO nano-structure is enhanced by the addition of silver attributed to doping-induced modification of surface properties (Ansari et al. 2014; Braiek et al. 2015; Hsu et al. 2014; Kumari et al. 2015; Patil et al. 2016; Sahu et al. 2012).

In this study, ZnO and ZnO@Ag core-shell nanorods were rapidly synthesized on ITO coated glass substrate for the first time using electrodeposition method without any organic surfactants or annealing at high temperature. The two-stage synthesis strategy is based on firstly aqueous electrodepositing of ZnO nanorods at low temperature and secondly in situ electrochemical etching of electrochemically deposited ZnO nanorods. Spectrochemical characterizations of the produced films have been done by using UV–vis absorption spectroscopy, UV-Visible Diffuse Reflectance Spectroscopy (DRS), photoluminescence spectroscopy (PL), X-ray photoelectron spectroscopy (XPS) and FT-IR spectroscopy (FTIR) analyses. The structural properties of the films have been investigated by using x-ray diffraction (XRD), scanning electron microscope (SEM), energy-dispersive X-ray (EDX), transmission electron microscopy (TEM) and atomic force microscopy (AFM). The produced films applied in the photocatalytic degradation of methylene blue and malachite green dyes as a model organic pollutant. Furthermore, photoelectrochemical (PEC; water splitting) performance of the produced films was investigated. The effects of production and operational parameters on the photocatalytic activity of the ZnO and ZnO@Ag core-shell nanorod films were investigated. The ZnO@Ag core-shell nanorods were found to exhibit improved photocatalytic performance in comparison with unmodified ZnO nanorods. The prepared nanorods grown on ITO substrates showed good photocatalytic activity and became reusable in the present studies because they did not show significant loss of activity related to

degradation of the dyes or splitting of photoelectrochemical water.

2. Material and Method

2.1. Materials

Zinc nitrate [Zn(NO3)2, Merck, min 99%], sodium nitrate [NaNO3, Carlo Erba Reagenti, min 99.5%], silver nitrate [AgNO3, Nalgene, min 99.5%], ethanol [C2H5OH, Merck, min %99]), acetone [C3H6O, Merck, min %99.8], malachite green [MG, Merck], methylene blue [MB, Merck] were purchased and were used without further purification. Millipore Milli-Q deionized water was used for preparation of all aqueous solutions.

2.2. Instrumentation

All electrochemical experiments were performed on a computer-controlled CHI660A electrochemical analyzer. The electrodeposition experiments were carried out in a three electrodes cell using a Pt wire (BAS-1033) as counter electrode, an Ag/AgCl (BAS-2052) as reference and an ITO coated glass (4-8 Ω, Delta Technologies) as working electrode. ITO substrates cleaned by using acetone, ethanol and deionized water in an ultrasonic bath for 10 min, respectively, before use. The spectroscopic experiments were carried out in a quartz cuvette (1 cm path length) using an Ocean Optics HR 4000 fiber optic UV–vis spectrophotometer in the wavelength range of 300–1000 nm. The UV-C tube lamp (15 W, length 41 cm, diameter 2.5 cm), model G15T8 (Philips, Holland) was used as the irradiation source (λ= 254 nm) located in a light infiltrated chamber. FT-IR measurements were carried out on a Perkin Elmer Spectrum 100 Fourier-Transform infrared (FTIR) spectrophotometer by using reflectance FTIR measurements system. The morphology and of the films was observed by SEM-ZEISS LS-10 scanning electron microscope (SEM) and NT-MDT atomic force microscope (AFM). The crystallinity of the deposited films was investigated by Shimadzu XRD-6000 X-Ray Diffraction (XRD). Photoluminescence (PL) spectroscopy of synthesized products was taken at room temperature on a HITACHI F-2700 fluorescence spectrophotometer using a Xe lamp with an excitation wavelength of 350 nm. UV-Visible Diffuse Reflectance spectra of the produced films were recorded in the range from

300 to 800 nm using a HITACHI U 3900 UV-visible diffuse reflectance spectrophotometer.

2.3. Preparation of the photocatalytic thin films

Two-step experimental methods consist of a low-temperature aqueous electrodeposition and an electrochemically etching has been applied to obtain electrodeposited ZnO nanorods on ITO coated glass substrate. In the first step, ZnO was electrodeposited on ITO substrates in an aqueous electrolyte containing 10 mM $Zn(NO_3)_2$ and 0.1 M $NaNO_3$ with a three-electrode electrochemical cell with ITO as the working electrode, a platinum wire counter electrode, and a Ag/AgCl reference electrode using an electrochemical Workstation. The electrodeposition was done by using constant potential electrolysis at -1.1 V and 80°C for 30 min under O_2 atmosphere. In the second step, electrochemically etching of electrodeposited ZnO nanorods was carried out by potentiostatically at 1.45 V in an aqueous electrolyte containing 0.1 M $NaNO_3$ for 3 min at 80 °C under O_2 atmosphere.

The fabrication strategy for the ZnO and ZnO@Ag core–shell arrays is shown in Fig1.
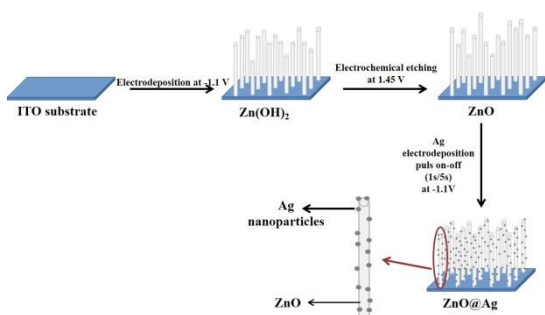
Figure 1. The fabrication strategy for the ZnO and ZnO@Ag core–shell arrays.

Usually, for the electrosynthesis of metal oxides, it is essential that the OH^- ions or O^- radicals should be produced around of the working electrode surface. Eg. 2 shows electrosynthesis of ZnO thin film is formed on the generation of hydroxide (OH^-) ions at the face of working electrode by electrochemical reduction of NO^{3-} in Zn^{2+} aqueous solution, as shown in Eq. (1) (Skompska and Zarebska 2014; Pradhan and Leung 2008; Udom et al. 2013).

$$NO^{3-} + H_2O + 2e^- \rightarrow NO^{2-} + 2OH^- \qquad (1)$$

The reduction of oxygen precursor at the interface of electrode was also occur to production of OH^- ions (Eq 2).

$$O_2 + 2H_2O + 4e^- \rightarrow 4OH^- \qquad (2)$$

When the Zn^{2+} ions in the aqeous solution react with OH^- ions around of working electrode surface, $Zn(OH)_2$ is formed at the surface of electrode (hydroxylation) (Eq 3),

$$Zn^{2+} + 2OH^- \rightarrow Zn(OH)_2 \qquad (3)$$
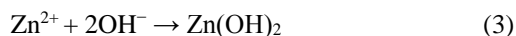
Finally, ZnO is spontaneously formed by dehydration of $Zn(OH)_2$ (Eq 4) when the temperature is controlled at 34°C and above (Lu et al. 2015).

$$Zn(OH)_2 \rightarrow ZnO + H_2O \qquad (4)$$

The size and morphology of ZnO nanostructures extremely adhere to on the experimental terms, especially the concentration of zinc nitrate, temperature and applied potential, which might change the reaction rate of the hydroxylation and dehydration.

By virtue of electrochemically generated acid (H^+) from anodic splitting of water the ZnO nanorod arrays were etched (Eq 5, 6) into the high surface-to-volume ratio of ZnO nanorod arrays (Xu et al. 2012).

$$2H_2O \rightarrow O_2 + 4H^+ + 4e^- \qquad (5)$$

$$ZnO + 2H^+ \rightarrow Zn^{2+} + 2e^- \qquad (6)$$
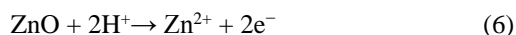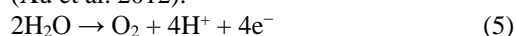
Finally, Ag was electrodeposited (Eq 7) onto the produced ZnO thin film for acquire Ag decorated ZnO film, using pulsing plating method in a solution including 10 mM $AgNO_3$, the chosen running voltage was -1.0 V and pulse on–off was 1 s/5 s.

$$Ag^+ + e^- \rightarrow Ag \qquad (7)$$

The applied potential and potential application time during electrodeposition of ZnO nanorods, potential application time during electrochemical etching and ratio of pulse on–off during Ag electrodeposition on ZnO nanorods were optimized to obtain maximum photocatalytic activity.

2.4. Measurements of photocatalytic activity

After the electrodeposition, the film was rinsed with deionized water several time and dried under air atmosphere. The photocatalytic decolorization of the dyes was performed in a quartz reactor. In the photocatalytic treatment of the dyes, a known concentration (samples were prepared in molar concentration) of the dye solution was taken in a quartz reactor. The photocatalytic thin film coated ITO coated glass substrate immersed to this dye solution. Then the reaction vessel was placed in a closed chamber with a UV source, so the solution could be illuminated from the side. The distance between the UV light source and the dye solution was 15 cm. The UV light intensity was measured 704 lux by using Smart Sensor Digital Lux Meter. Before irradiation, the photocatalytic thin film coated substrate immersed solution was stored for 60 min in dark conditions until adsorption-desorption equilibrium was established without stirring. The lamp was switched on to initiate the photocatalytic decolorization reaction. The photocatalytic decolorization of organic dyes was investigated at room temperature in the presence/absence of different catalysts under irradiation/dark for given times. To check the photocatalytic activity of the films, the decomposed dye solution was measured after regular time intervals of 15 min using UV-vis absorption spectra. A calibration graph based on Beer-Lambert's law was obtained by plotting the absorbance against the concentration of dye in solution. The concentrations of the dyes were calculated by calibration curves.

2.5. Photoelectrochemical measurements

To investigate the photoelectrochemical reply of the ZnO and ZnO@Ag core-shell nanorod films on ITO coated glass linear sweep voltammetry (LSV) and chronoamperometry experiments were done under atmospheric conditions in the dark and under UV light irradiation in a 0.5 M NaNO3 aqueous solution at room temperature. Photoelectrochemical measurements were performed in an electrochemistry workstation (CH Instruments 660A) with a three-electrode system. The ZnO and ZnO@Ag nanorod arrays were used as the working electrode, an Ag/AgCl rod was the reference electrode, and a platinum wire was the counter electrode. The total effective area of the working electrode was 0.25 cm2. The water splitting photoelectrode was illuminated by using UV-C tube lamp. Current–voltage (I–V)

curves were measured under dark and visible light irradiation at a scan rate of 10 mV/s over a potential range of −0.9 to 0.9 V. Amperometric I-t curves of ZnO and ZnO@Ag nanorod arrays were recorded under chopped light irradiation (light on or off cycle: 100 s) at an applied potential of 0.6 V vs. Ag/AgCl.

3. Results

3.1. Characterization of the produced films

3.1.1. Crystallographic properties

XRD analysis was performed to investigate the crystal structure of the produced photocatalytic films. Fig2 shows the XRD pattern of the electrochemically synthesized ZnO (before and after electrochemical etching) and Ag decorated ZnO films.
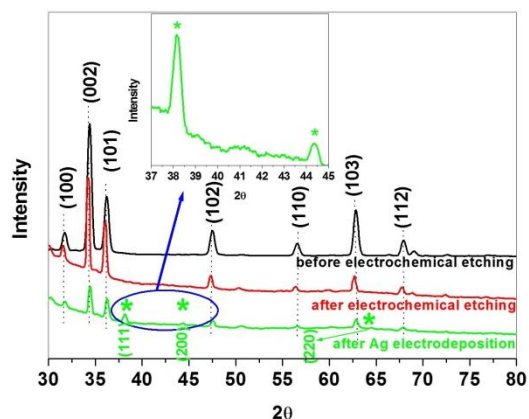
Figure 2. XRD patterns of the produced films on ITO coated glass substrate.

The strong and sharp peaks seen on the XRD patterns confirms that the prepared samples have complete crystalline structure. The structure of ZnO nanorods was not affected by the accumulating of Ag onto ZnO/ITO electrode. The characteristic peaks of the (100), (002),(101), (102), (110), (103), (200), (112), and (201) planes of hexagonal wurtzite ZnO are clear at 2θ values of 31.74°, 34.38°, 36.22°,47.48°, 56.54°, 62.78°, 67.87°, 69.01°, 72.47° respectively (JCPDS 36-1451) (Ansari et al. 2014). As can be shown this figure, some new peaks marked with "*" after electrodeposition Ag on to ZnO/ITO electrode was obtained, which indicates the Ag electrodeposition on the ZnO structure. Furthermore, comparing the peak intensity of the

diffraction patterns of ZnO and the ZnO@Ag nanorods, it is evident that the peak intensity of the ZnO nanorods has been reduced in the ZnO@Ag nanorods's XRD spectrum. This can indicate that the ZnO NPs are covered with another material. After Ag accumulation to ZnO nanorods, crystalline metallic Ag is observed by XRD. Ag decorated ZnO nanorods shows that the characteristic peaks of the (111), (200) and (220) planes of cubic Ag are clear at 2θ values of $38.117°$, $44.30°$ and $64.45°$ respectively (JCPDS 04-0783) (Ansari et al. 2013). The Ag XRD peak is relatively weak and broad, as shown in the inset in Fig 2, indicating a small size and well dispersed Ag at the surface of ZnO nanorods. XRD patterns showed a hexagonal wurtzite structure both for ZnO and Ag electrodeposited ZnO films. Since the XRD pattern of the Ag decorated ZnO catalyst shows no significant shifting the 2θ values of the characteristic peaks as a result of the accumulating process, the introduction of Ag does not alter the crystal structure. These demonstrate that cubic structured Ag is produced after the second electrodeposition steps and shows the stability of the two compounds during the synthesis process. These findings confirm the successful production of ZnO @ Ag core-shell nanorods. To verify the ZnO@Ag structure, the morphology and chemical composition of the produced samples was examined by SEM, AFM and EDX analyzes.örnek alanlardaki dağılımı(%)

3.1.2. Morphological properties

The morphology-controlled synthesis of ZnO nanostructure is of great interest for future ZnO nanomaterial applications. The morphologies of as electrochemically grown films were characterized using SEM and the representative SEM images of the films (before electrochemical etching, after electrochemical etching, and after Ag electrodeposition) are shown in Fig3. The insets in Fig 3 show high magnification SEM images of the morphology.
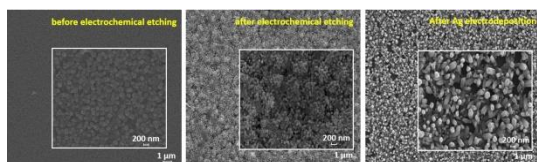
Figure 3. SEM image of the produced films on ITO coated glass substrate.

It can be seen this figure, three of the thin films have the rough surfaces and consisted of the compact, uniform and nanorod arrays. The obtained nanorod arrays produced on ITO substrate in the first-step electrodeposition were mainly 160–110 nm in diameter and showed high orientation perpendicular to the substrates. After electrochemical etching for 3 min by generated acid (H⁺) from anodic splitting of water, the surface-to-volume ratio of ZnO nanorod arrays was increased, as shown in Fig 3. Although the morphology of thin films was not significantly affected by Ag deposition, it caused an increase in the size of ZnO @ Ag nanorods compared to pure ZnO nanorods (Fig3). The diameters of ZnO nanorods were about 52-84 nm in ZnO film after electrochemical etching and the diameters of the rods increased about 74-148 nm with the Ag decorating.

Change in the surface morphology of the ZnO thin films after Ag deposition was also investigated using an AFM analysis. Fig4 show the AFM 2D- and 3D-images of the ZnO films before and after Ag deposition (scan area 20 µm × 20 µm), respectively.
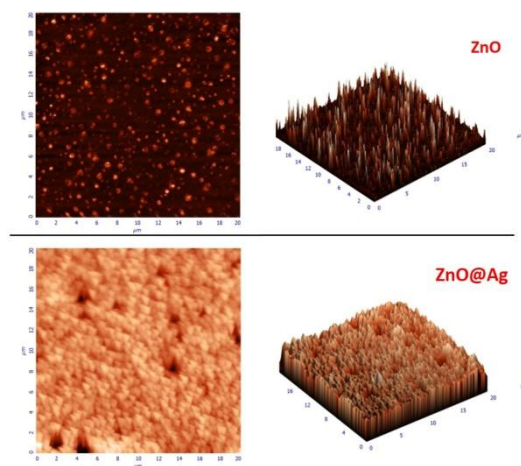
Figure 4. AFM image of the ZnO and ZnO@Ag films on ITO coated glass substrate.

AFM images also confirm that the ZnO and ZnO@Ag films are nanorod array. Furthermore, after Ag deposition, the surface roughness of the film significantly changed.

3.1.3. Spectroscopic properties

Film composition and spectroscopic properties plays a major role in the photocatalytical and

photoelectrochemical activity of the produced films. To verify the chemical composition and spectroscopic properties of the ZnO and ZnO@Ag films, FTIR, EDX, PL and DRS measurements were carried out. Fig.5 shows the FTIR spectra of the ZnO and ZnO@Ag films.
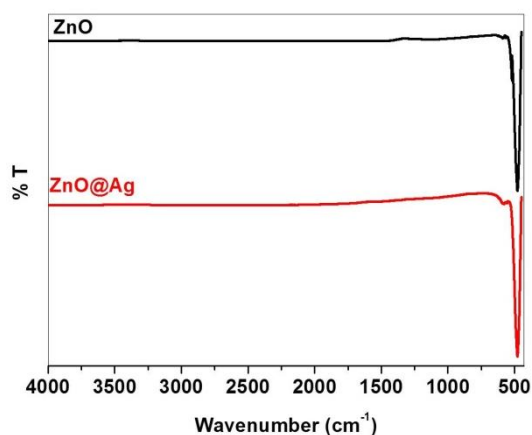
Figure 5. FTIR spectra of the ZnO and ZnO@Ag films on ITO coated glass substrate.

Both of the films, one strong absorption bands correspond to the characteristic stretching mode of Zn-O was observed at 479 cm^{-1} (Braiek et al. 2015; Zhang et al. 2012). After Ag deposition, a new absorption peak was observed at 583 cm^{-1} which is indicates the presence of the Ag nanoparticles in the ZnO@Ag nanorod arrays.

The energy dispersive X-ray spectroscopy (EDX) mapping of the grain of the ZnO and ZnO@Ag nanorods are shown in Fig6. Elemental zinc, oxygen, and silver are detected, and the corresponding weight and atomic percentages of the produced photocatalysts were also given in insets of Fig6.
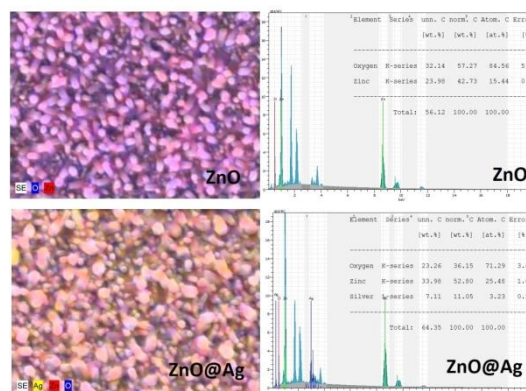
Figure 6. SEM-EDX mapping, EDX spectra and chemical composition of the ZnO and ZnO@Ag nanorod films

Zn, O, and Ag elements have been found in the ZnO@Ag nanorods while Zn and O elements have been found by EDX measurements. Quantitative analysis shows that the ZnO nanorods is not stoichiometric ratio of Zn and O because the oxygen element has two sources that ZnO film and oxygen in the ITO coating under nanorods. Furthermore, In and Sn elements also found EDX spectra of three films due to the ITO substrate. The homogeneous distributions of Zn, Ag and O shown in Fig6, indicating that the ZnO core nanorods are fully covered with Ag shell. The Ag content of the ZnO@Ag nanorods arrays shown in inset of Fig6 is about 3.23 atom % revealed by EDX. Chemical atomic wt. % compositional analyses for zinc, oxygen and silver estimated from EDX spectrum were well supported the formation of Ag over ZnO nanorods. The FTIR and EDX results were in good alignment with the XRD result. These results indicate that ZnO@Ag nanorods have highly crystalline structure with a tiny and uniform dispertion of Ag nanoparticles at the ZnO nanorod surface, which is beneficial for the photocatalytic activities. The result confirms again that the ZnO@Ag core-shell nanorod arrays has been successfully fabricated by the two step electrochemical method.

The optical performance and band gap energy perform a significant role in the photocatalytic process. The optical performance of ZnO and the ZnO@Ag nanorod arrays was determined by the UV–vis diffuse absorption spectra, which are displayed in Fig7.
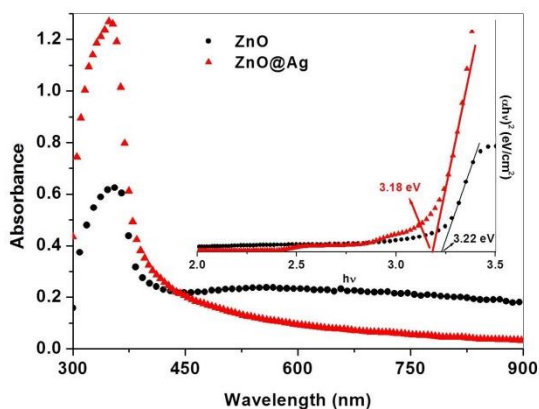
Figure 7. UV-visible diffuse absorption spectra of the ZnO and ZnO@Ag core-shell nanorod films. The inset shows the plots of $(\alpha h\upsilon)^2$ versus $h\upsilon$ of these films

As shown in Fig7, the absorption of the films mainly focusing on the UV zone and the absorption of the Ag@ZnO nanorods was higher than that of pure ZnO nanorods. A hard peak centered at about 350 nm corresponding to the ground excitonic state of ZnO (Li et al. 2011). This exciton peak comply to the highly crystalline nature of the nanorods with surface defects. The insets in Fig7 shows the plot of $(\alpha h\upsilon)^2$ versus $h\upsilon$ for the ZnO and the ZnO@Ag nanorod arrays and demonstrates that the optical band gap of the ZnO nanorods is 3.22 eV which is smaller than the theoretical value of bulk ZnO (3.37 eV) (Bu 2015; Rahman et al. 2015; Yoo et al. 2015; Zhang et al. 2012; Zulkifli et al. 2015). The possible reason could be due to structural defects arising during the preparation of the material. As it can be seen from inset of Fig7, the band gap of the ZnO@Ag nanorods is slightly smaller than that of pure ZnO nanorods. This is attributed to the no significant interfacial electron coupling between ZnO and Ag during the electrochemical deposition process.

ZnO has been extensively studied as a photocatalyst for environmental remediation due to its low cost, excellent electrochemical stability and high electron mobility. But, the quick recombination of photoexcited electrons and holes decreases its photocatalytic performance. Thus, achieving effective charge separation and blocking electron-hole recombination of these nanostructures is a key factor in maintaining the high photoactivity of nanoscale photocatalysts (Braiek et al. 2015). In a photocatalytic process, the separation and recombination of photoinduced

charge carriers are competitive routes and the photocatalytic performance is effective when the recombination between them is prevented. The efficiency of the recombination can be measured by the luminescence intensity. The PL evaluations were performed to determine the charge recombination and migration efficiency of the produced films because the photocatalytic activity is related closely to the PL intensity and the recombination rate of photo excited electrons and holes. Fig8 shows the PL spectra of the ZnO and the ZnO@Ag core-shell nanorod arrays measured at an excitation wavelength of 350 nm.
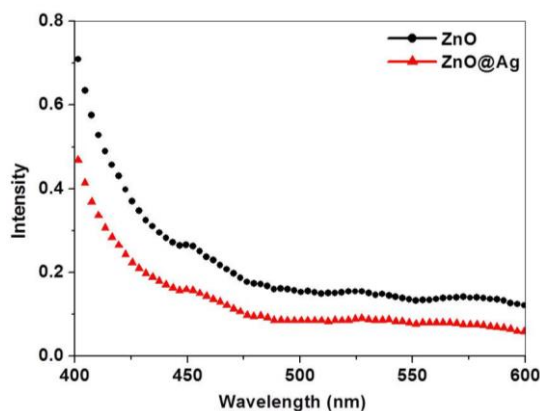
Figure 8. PL spectra of the ZnO and ZnO@Ag core-shell nanorod films

The emission intensity of the PL spectrum of the ZnO@Ag core-shell nanorod arrays was lower than that of ZnO nanorod arrays suggesting that the anchoring of Ag decoration could quench the fluorescence from the ZnO nanorods and prolong electron-hole pair lifetime (Ansari et al. 2013). This decrease can be attributed to the electron trapping effect of Ag, which acts as an acceptor species and inhibits the recombination of charge carriers on ZnO (Bechambi et al. 2015). A lower density of photoluminescence means a lower electron-hole recombination rate and thus a longer lifetime of the photogenerated carriers. Effective charge separation and inhibition electron-hole recombination with the Ag nanostructure is generally favorable to enhance the photocatalytic activity of ZnO (Chen et al. 2013). The PL spectra showed that the decoration of the Ag nanostructures to the ZnO nanorods could effectively inhibit the recombination of electrons and holes during the photocatalytic reaction under UV light irradiation.

3.2. Photocatalytic activity of the produced films

Methylene blue and malachite green are organic dyes used in the various industries like printing, textile and photographic. When discharged into environment they are dangerous to aquatic life and, in many cases, shows carcinogenic effect on humans and animals (Gülce et al. 2013). So, degradation of these organic dyes is of great importance to water purification and conservation. These dyes are selected as model compound for investigation of photocatalytic activity of produced ZnO and ZnO@Ag core-

shell nanorod arrays. The photocatalytic activity of the produced films were evaluated by monitoring the change in concentration of the dyes as a function of UV irradiation time. The control experiment exposes aqueous solution of MB and MG to UV light without photocatalyst, in which no detectable degradation in the dye solution was observed.

Fig9 shows the change in UV–vis optical absorption spectra of MB and MG dyes by ZnO and ZnO@Ag core-shell nanorod films on ITO coated glass substrates under UV irradiation for different time intervals.
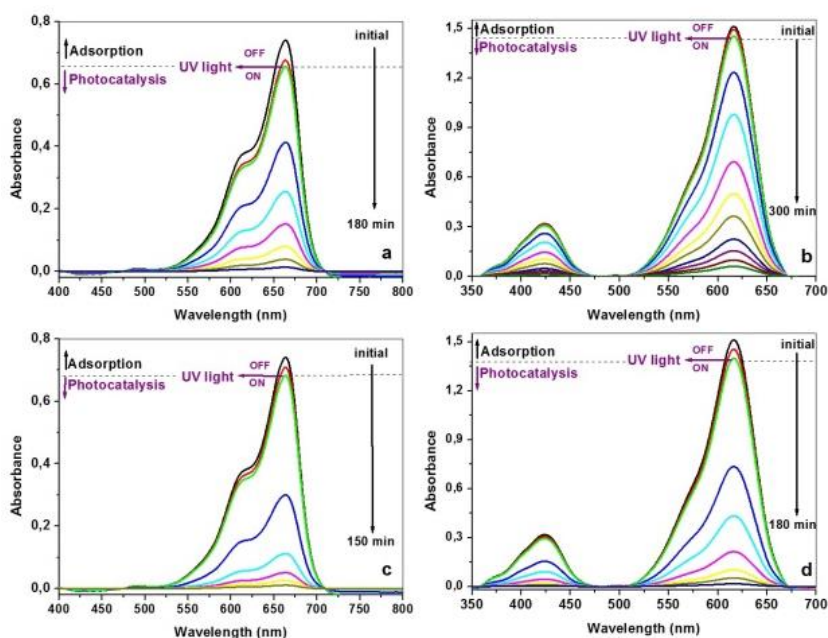
Figure 9. The change in UV-vis absorption spectra in the presence ZnO nanorod film of a) MB, b) MG and in the presence the ZnO@Ag core-shell nanorod film (c) MY, (d) MG under UV light irradiation (initial concentration of dyes: 1×10^{-5} M).

The decrease of the absorption band intensities of the dyes indicated that dyes have been degraded by the ZnO and ZnO@Ag core-shell nanorod photocatalyst. As can be seen this figure, the disappearance of the characteristic band of MB and MG dyes after 150 min. and 180 min. respectively, under UV light irradiation indicates that MB and MG dyes have been degraded completely by ZnO@Ag core-shell nanorod film (Fig9c and 9d). It can be seen Fig9a and 9b, the

disappearance of the characteristic band of the dyes not occur for same time intervals when ZnO film was used as photocatalyst.

The concentrations ratio (C/C_0) is calculated in order to evaluate the degradation efficiency of the dyes. Fig10 shows the concentrations ratio versus irradiation time for the MB and MG dyes solutions in the presence of the ZnO and ZnO@Ag core-shell nanorod films.
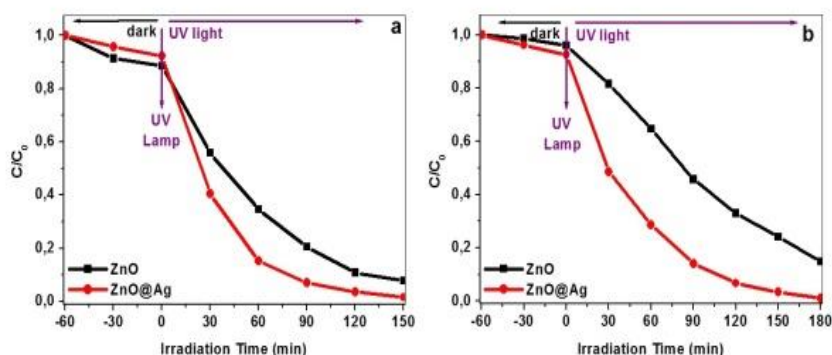
Figure10. The concentrations ratio versus irradiation time for the a) MB, b)MG dyes solutions in the presence of the ZnO and ZnO@Ag core-shell nanorod films under UV light irradiation.

Before irradiation, the photocatalytic thin film coated substrate immersed solution was stored for 60 min in dark conditions to understand the effect of UV illumination. As seen Fig10a and 10b, the decolorization efficiencies are 9.34% and 5.24% for MB and MG dyes respectively under dark conditions in the presence of the ZnO nanorod film due to adsorption mechanism. The decolorization efficiencies of MB and MG dyes are 7.18% and 6.91% respectively under dark conditions when the ZnO@Ag core-shell nanorod film used as catalyst. The lamp was switched to study the effect of UV irradiation on the catalyst-dye interaction. As shown in Fig10a-b, the degradation of MB using the ZnO@Ag core-shell nanorod film is 100%, while the ZnO nanorod film 83%, for 150 min irradiations. The decolorization efficiency of MG are 100% and

84% for the ZnO@Ag core-shell and ZnO nanorod films respectively, for 180 min irradiations (Fig10b). It is clearly seen that the presence of Ag the ZnO matrix accelerates the photocatalytic process.

In general, the kinetics of photocatalytic degradation of organic pollutants on the semiconducting materials has been established and can be described well by the apparent first order reaction $\ln(C_0/Ct)=k_{appt}$, where kapp is the apparent rate constant, C_0 is the concentrations of dyes after darkness adsorption for 60 min and C_t is the concentration of dyes at time t. Fig11 shows the relationship between UV illumination time and the degradation rate of dyes.
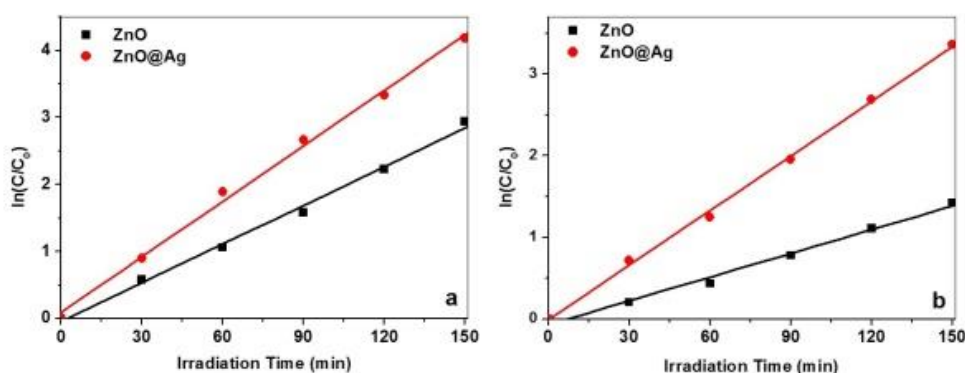
Figure 11. The relationship between UV illumination time and the degradation rate of a)MB, b)MG.

The linear correlation of the plots of $\ln(C_0/C_t)$ versus time suggested a pseudo first-order reaction for the both dyes. The appeared reaction

rate constants calculated using the linear extrapolations. The activity of synthesized film photocatalysts under UV light can be evaluated by

comparing the apparent rate constants (kapp) listed in Table 1.

	Methylene Blue				Malachite Green			
	ZnO		ZnO@Ag		ZnO		ZnO@Ag	
	k_{app} (min^{-1})	R^2	k_{app} (min^{-1})	R^2	k_{app} (min^{-1})	R^2	k_{app} (min^{-1})	R^2
1. usage	0.5764	0.9949	0.8283	0.9963	0.2909	0.9911	0.6693	0.9983
2. usage	0.5558	0.9891	0.7874	0.6916	0.2891	0.9900	0.6591	0.9979
3. usage	0.5513	0.9881	0.7652	0.9949	0.2875	0.9894	0.6492	0.9973
4. usage	0.5445	0.9881	0.7459	0.9987	0.2798	0.9829	0.6419	0.9959
5. usage	0.5264	0.9897	0.7432	0.9959	0.2729	0.9826	0.6369	0.9952

As can be seen in Table 1, the photocatalytic activity of the ZnO@Ag core-shell nanorod arrays is higher than that of ZnO nanorod arrays for both dyes. The enhanced photocatalytic activity of the ZnO@Ag core-shell nanorod film compared to the pure ZnO nanorod film indicates that the Ag decoration improve the photocatalytic activity of the ZnO nanorods for the effective degradation of dyes and organic compounds when exposed to UV light. The degradation rate of MB and MG is 1.4 and 2.3 times greater on the ZnO@Ag core-shell nanorods compared to the rate with pure ZnO nanorods, respectively.

To evaluate the photocatalytic stability of the ZnO@Ag core-shell and ZnO nanorod films, it was used for several photocatalytic runs using in each measurement a new dye solution with the same initial concentration under UV light irradiations for the both dyes. After the first run, the film coated ITO substrate was separated and used immediately for further runs without any treatment. Fig12 represent the cyclic usage of the produced photocatalyst films for degradation of the MB and MG dye solutions under UV light irradiation.
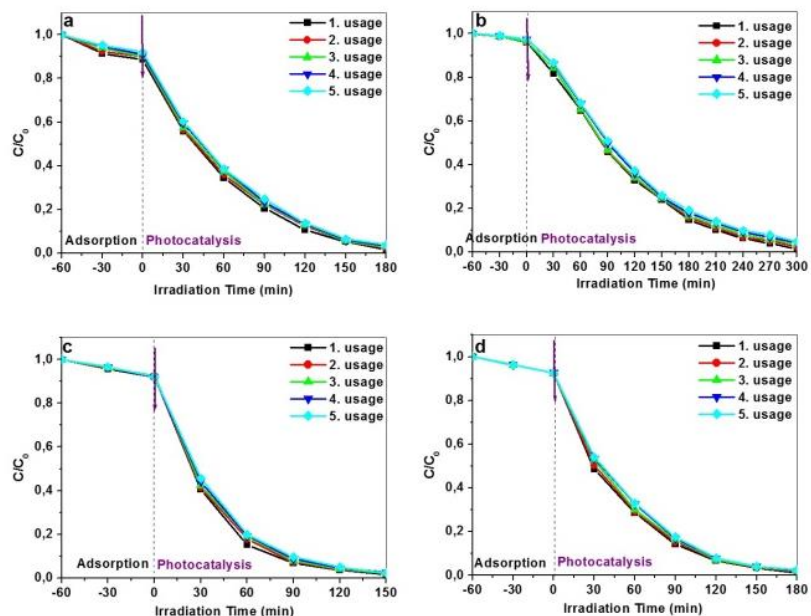
Figure 12. Effect of number of runs on the degradation of dyes in the presence ZnO nanorod film (a) MY, (b) MB and in the presence the ZnO@Ag core-shell nanorod film (c) MY, (d) MG (initial concentration of dyes: 1×10^{-5} M).

It has been confirmed that the both films maintains its good photocatalytic activity even after five cycles. Furthermore, Ag deposition has significantly increased the photocatalytic stability of the produced nanorod film.

The photocatalytic stability of the produced films is confirmed by comparing the apparent rate constants (k_{app}). The results in Table 1 show that the film photocatalyst is reusable and that it can also maintain relatively high activity after several experimental runs. After five recycles for the photodegradation of the dyes, the photocatalyst did not exhibit any significant loss of activity, as shown in Fig12 and Table 1, confirming the ZnO@Ag core-shell and ZnO nanorod films are not photocorroded during the photocatalytic oxidation of the pollutant molecules.

3. 3. Photoelectrochemical performance of the produced films

To investigate the photoelectrochemical performance of the ZnO and ZnO@Ag core-shell nanorod films on ITO coated glass in water splitting, we also performed LSV in dark and under UV light illumination as shown in Fig13a.
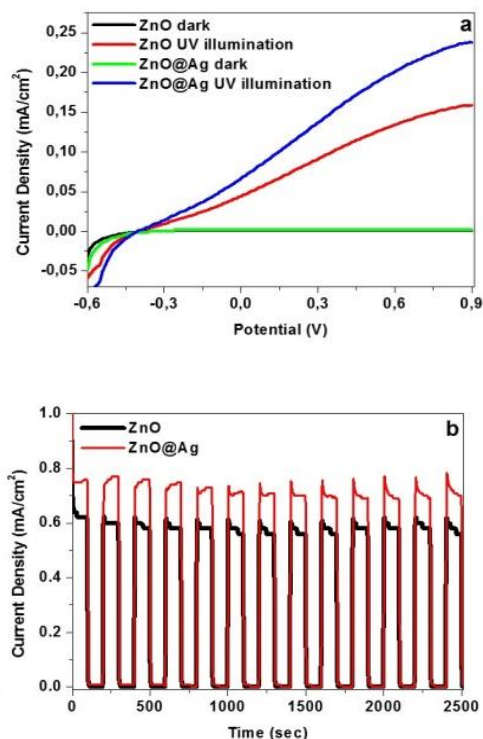
Figure 13. Photoelectrochemical performance of the ZnO and ZnO@Ag core-shell nanorod films on ITO coated glass in water splitting a) LSV in dark and under UV light illumination b) current density response to on–off cycling with total test duration of 2500 s

A neglible current was observed on both of the produced electrodes under dark conditions. Under illumination, the current densities of the electrodes increased with the applied potential. The ZnO nanorod film electrode exhibited a photocurrent of only 0.1560 mA cm^{-2} at 0.8 V versus Ag/AgCl. In the presence of ZnO@Ag core-shell nanorod film electrode, the current density indicates a significant increasing up to 0.2396 mA cm^{-2} at the same potential. The photocurrent of ZnO@Ag core-shell nanorods enhanced as compared to ZnO nanorods which showed that the Ag decoration on ZnO can effectively increase the photo conversion efficiency. The increment of photocurrent also indicates the enhance of photoinduced carriers transport rate and the improvement of photogenerated electron-hole pair separation. Also, the extent of electron-hole recombination in the ZnO and ZnO@Ag core-shell nanorod films on ITO coated glass were also supported by PL results (Fig8). This result clearly shows that the Ag decoration can efficiently depress the recombination of photogenerated electron-hole pairs and increased the photocatalytic performance of the ZnO@Ag core-shell nanorods (Ansari et al. 2013). According to these results, we concluded that the ZnO@Ag core-shell nanorods could serve as efficient materials for the enhancement of photocurrent. The excellent photoelectrochemical properties can be attributed to the Ag/ZnO heterojunction function to reduce the recombination of photo-generated electrons and holes.

Both photoelectrodes (the ZnO and ZnO@Ag core-shell nanorod films on ITO coated glass) were illuminated at intervals (+0.6 V vs. Ag/AgCl) in several cycles to assess the repeatability of the reproducibility of their photoresponses as well as the stability of the device to oxidation. The current density response, which corresponds to the on-off cycle with a total test duration of 2500 s, is presented in Fig13b. From this figure, we can observe that both photoelectrodes cause an instantaneous change of current in the illumination. After the light turned off, the current was almost instantly attracted to the original values. These results showed the stability of both thin films. Besides, we can note from Fig13b that the photocurrent density produced by ZnO@Ag core-shell nanorod film electrode is higher than that measured on ZnO nanorod film.

These results demonstrate that ZnO@Ag core-shell nanorods have better photo-electrochemical activity than pure ZnO nanorods under UV illumination. In this case, the coupling of Ag and ZnO nanorods could transfer electrons from Ag into ZnO for their suitable conduction of band potentials. The improved ZnO photocurrent density after the addition of the Ag nanoparticles can be ascribed to the enhanced separation of electron–hole pairs in the ZnO@Ag core-shell nanorod arrays (Hsu and Chang 2014). This result is in good agreement with that obtained in the photocatalytic activity. It has been reported that surface properties are modified by decorating the surface of ZnO with Ag or different nanostructure. This decoration also enhances the interfacial charge-transfer kinetics between the metal and semiconductor (Ansari et al. 2013; Patil et al. 2016). This improves the separation of the photogenerated electron-hole pairs and transport to their respective electrodes. The successful transport of charge carriers has resulted in the enhanced photoelectrochemical activity of the ZnO photoanode.

3.4. Possible Mechanisms in Enhancing Photocatalytic Activity

Photocatalysis is the acceleration of a photoreaction by the action of a catalyst; the catalyst interacts with a substrate in its ground state or excited state and/or with a primary photoproduct. A photocatalyst uses the characteristics of semiconductors in a photochemical reaction to decompose organic pollutants (Ansari et al.2013; Chen et al. 2013; Hsu and Chang 2014). The semiconductor possesses a band gap which separates the top of the electron-filled valence band (VB) from the vacant conduction band (CB). When ZnO is irradiated with light that is greater than the band gap energy, electrons in the valence band (VB) moves to the conduction band (CB) leading to the producing an electron(e) and a positive hole (h+), in the CB and VB, respectively. The electron (e) and hole (h+) both migrate to the catalyst surface to recombine or preferably facilitate a redox reaction with compounds absorbed on the catalyst. The combination of the positive hole(h+) with water and/or hydrogen peroxide (H$_2$O$_2$) produces hydroxyl radicals (OH•), powerful oxidants that oxidize the organic compounds in the photocatalytic system. Simultaneously, oxygen molecules absorbed on the photocatalyst

are reduced by the electrons in the conduction band. During the photocatalytic process, reactions with oxygen (O_2) causes superoxide radicals (O_2^-) and other reactive oxygen species to form. Superoxide and H_2O_2 act as electron acceptors, or, for H_2O_2, a direct source of hydroxyl radicals due to hemolytic scission, and help the oxidation of organic and inorganic electron donors (Bechambi et al. 2015; Skompska and Zarebska 2014; Xu et al. 2012). The modification of photocatalyst with several materials increased photocatalytic activity. The mechanisms of the enhanced photocatalytic activity of the photocatalyst modified with noble metal have been proposed by several researchers (Ansari et al. 2014; Ansari et al. 2015; Chen et al. 2013). In the case of metal modification in nanomaterials, metal modifier can change the photophysical properties. From the study, it can be seen that the decoration of Ag on ZnO nanorod arrays enhances the photocatalytic activity in photodegradation of the dyes and photoelectrochemical performance in water splitting of the ZnO nanorod film. It is assumed that decorated Ag on the ZnO nanorods can act as electron-hole separation centers. The photocatalysis test results demonstrate that the separation of photogenerated electron-hole pairs is enhanced by Ag/ZnO interfaces present in the ZnO@Ag nanorod arrays and thus the photocatalytic activity improves. The high photoactivity of ZnO@Ag core-shell nanorod arrays was also attributed to the higher UV light absorbance. These comments also confirmed the UV-visible diffuse reflectance and PL spectroscopy results. The photocatalytic reaction process of the novel ZnO@Ag nanorod arrays is proposed as follows and shown in Fig14.
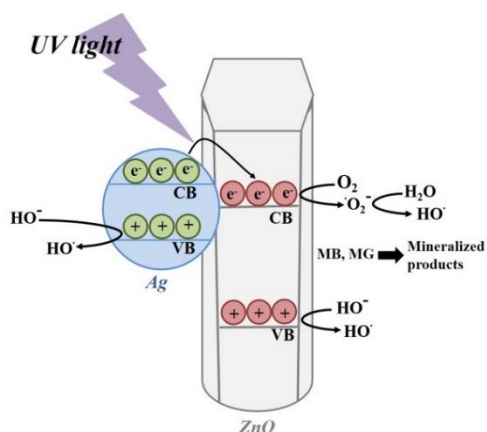
Figure 14. The photocatalytic reaction process of the ZnO@Ag nanorod

(1) Both the ZnO nanorods and the Ag nanoparticles act as electron and hole sources. When the Ag nanoparticles absorb photons of energy greater than or equal to the band gap, photoelectrons may be promoted from the valence band (VB) to the conduction band (CB), leaving behind same amount of electron vacancies or holes in the VB.

(2) Since the energy level of the bottom of the CB of Ag nanoparticles is higher than the energy level of the ZnO nanorods, the photoelectrons could transfer from Ag to ZnO driven by the energy difference. The Ag nanostructures act as mediator for transferring the photoelectrons. Thus, the recombination of photoelectrons and holes prior to the superoxide activation process is avoided and the photoinduced generation of electron-hole pairs will continue. The Ag nanoparticles on ZnO nanorods which acts as electron sinks can trap the photogenerated electrons from the semiconductor. Therefore, the photogenerated charge carriers can be separated effectively and improve the photocatalytic activity of Ag-deposited ZnO under UV irradiation (Ansari et al. 2015; Bechambi et al. 2015; Chen et al. 2013; Xu et al. 2012).

(3) The photoinduced holes may react with surface-bound H_2O or OH^- to produce the hydroxyl radical species ($\cdot OH$), which is an extremely strong oxidant to most organic chemicals. Free electrons may be picked up by oxygen molecules dissolved in the solution to generate superoxide radical anions ($\cdot O_2^-$), which are the active species for the overall photocatalytic oxidation (Hsu and Chang 2014; Xu et al. 2012).

4. Discussion and Conclusions

ZnO nanomaterials has several advantages such as low cost, excellent electrochemical stability and high electron mobility for photocatalytical applications. However, its main disadvantage is that its photocatalytic activity is hindered by rapid recombination of photoexcited electrons and holes. Hence, ensuring the efficient charge separation and inhibition of electron-hole recombination of the ZnO nanostructures is the key factor for preserving its high photocatalytic activity. In this study, Ag deposited ZnO core-shell nanorod films synthesized by using electrodeposition method on ITO coated glass

substate and their photocatalytic activity and photoelectrochemical performance were evaluated. The characteristic properties of pure and Ag doped ZnO were investigated by using XRD, SEM, AFM, EDX, FTIR, PL and UV-vis diffuse reflectance. The photocatalytic activity was investigated by degradation of MB and MG dyes under UV light irradiation. The modification of Ag was importantly increased the photocatalytic activity and stability. The UV-visible diffuse reflectance, PL spectroscopy, photocatalytic and photoelectrochemical experiments showed that decoration Ag nanostructures to the surface of ZnO nanorods has significantly increased the photocatalytic activity and photostability of the produced nanorod films. The Ag nanostructures at the surface of ZnO act as mediator for transferring the photoelectrons and effectively inhibit electron-hole recombination during the photocatalytic reaction under UV light irradiation. The photocurrent of ZnO@Ag core-shell nanorods enhanced as compared to ZnO nanorods which indicated that the Ag decoration on ZnO could effectively improve the photoconversion efficiency. Increase of photoinduced carriers transport rate and the improvement of photogenerated electron-hole pair separation can also be observed with the enhancement of photocurrent.

In conventional photocatalytic processes, suspended semiconductor materials are used in the wastewater treatment. The most important disadvantage of such applications is the necessity of using additional separation procedures to remove the entrails used as photocatalysts again after the photocatalytic reaction. If the appropriate films are used as photocatalyst no further separation and purification process is required. The photocatalysts produced in this work are films on the surface, these film photocatalyst is produced no secondary pollution and no further separation and purification process is required. The same photocatalytic film can be used numerous times which leads to a reduction in cost for sustained wastewater treatment.

The results we present suggest that the production of ZnO@Ag nanorod films without any organic surfactants or high annealing temperature is an economical and effective process for the production of efficient photocatalytic film on an appropriate conducting surface, at larger scale, that is suitable for degrading dyes in wastewaters.

References

Ansari, S.A., Khan, M.M., Ansari, M.O., Lee, J., Cho. M.H. (2013). Biogenic Synthesis, Photocatalytic, and Photoelectrochemical Performance of Ag–Zno Nanocomposite. The Journal of Physical Chemistry C 117(51), 27023-30.

Ansari, S. A., Khan, M.M., Lee, J., Cho, M.H. (2004). Highly Visible Light Active Ag@Zno Nanocomposites Synthesized by Gel-Combustion Route. Journal of Industrial and Engineering Chemistry, 20 (4), 1602-1607.

Bechambi, O., Chalbi, M., Najjar, W., Sayadi, S. (2015). Photocatalytic Activity of Zno Doped with Ag on the Degradation of Endocrine Disrupting under Uv Irradiation and the Investigation of Its Antibacterial Activity. Applied Surface Science, 347, 414–20.

Braiek, Z., Brayek, A., Ghoul, M., Taieb, S. B., Gannouni, M., Ben Assaker, I., Souissi, A., Chtourou. R. (2015). Electrochemical Synthesis of Zno/In2s3 Core–Shell Nanowires for Enhanced Photoelectrochemical Properties. Journal of Alloys and Compounds, 653, 395-401.

Bu, I.Y. (2015). Enhanced Photocatalytic Activity of Sol–Gel Derived Zno Via the Co-Doping Process. Superlattices and Microstructures, 86, 36–42.

Chandrasekhar, M., Nagabhushana, H., Vidya, Y.S., Anantharaju, K.S., Sharma, S.C., Premkumar, H.B., Prashantha, S.C. et al. (2015). Synthesis of Eu3+-Activated Zno Superstructures: Photoluminescence, Judd–Ofelt Analysis and Sunlight Photocatalytic Properties. Journal of Molecular Catalysis A: Chemical, 409, 26-41.

Chen, L., Tran. T., Huang, T.C., Li, J., Yuan, L., Cai. Q. (2013). Synthesis and Photocatalytic Application of Au/Ag Nanoparticle-Sensitized Zno Films. Applied Surface Science, 273, 82-88

Chikoidze, E., Nolan, M., Modreanu, M., Sallet, V., Galtier, P. (2008). Effect of Chlorine Doping on Electrical and Optical Properties of Zno Thin Films. Thin Solid Films 516(22), 8146-49.

El Amiri, A., Moubah, R., Lmai, F., Abid, M., Hassanain, N., Hlil, E.K., Lassri, H. (2016). Probing Magnetism and Electronic Structure of Fe-Doped Zno Thin Films. Journal of Magnetism and Magnetic Materials 398, 86-89.

Fabbri, B. , Gaiardo, A., Giberti, A., Guidi, V., Malagù, C., Martucci, A,. Sturaro, M., et al. (2016). Chemoresistive Properties of Photo-Activated Thin and Thick Zno Film. Sensors and Actuators B: Chemical 222, 1251–56.

Ge, C., Li, H., Li, M., Li, C., Wu, X., Yang, B. (2015). Synthesis of a Zno Nanorod/Cvd Graphene Composite for Simultaneous Sensing of Dihydroxybenzene Isomers. Carbon, 95, 1-9 .

Gülce, H., Eskizeybek, V., Haspulat, B., Sarı, F., Gülce, A., Avcı. A. (2013). Preparation of a New Polyaniline/Cdo Nanocomposite and Investigation of Its Photocatalytic Activity: Comparative Study under Uv Light and Natural Sunlight Irradiation. Industrial & Engineering Chemistry Research, 52(32), 10924-34.

Habibi, M.H., Shojaee, E. (2015). Fabrication and Characterization of Cobalt Sensitized Nanostructure Zinc Oxide Thin Film Coated on Glass by Sol-Gel Spin Coating Using Trans-Bis(Acetylacetonato)-Bis(4-Methylpyridine)Cobalt(Iii). Synthesis and Reactivity in Inorganic, Metal-Organic, and Nano-Metal Chemistry, 45 (11), 1642-46.

Hsu, M.H., Chang, C.J. (2014). Ag-Doped Zno Nanorods Coated Metal Wire Meshes as Hierarchical Photocatalysts with High Visible-Light Driven Photoactivity and Photostability. Journal of Hazardous Materials 278, 444-53.

Kaneva, N.V., Dimitrov, D.T., Dushkin, C.D. (2011). Effect of Nickel Doping on the Photocatalytic Activity of Zno Thin Films under Uv and Visible Light. Applied Surface Science 257, 8113–20.

Kang, S.H., Ahn, D.B., Kim, H.J., Kim, H.G., Lim, H.S., Chang, W.H., Lee, Y.S. 88 (2006). Structural, Electrical, and Optical Properties of P -Type Zno Thin Films with Ag Dopant. Applied Physics Letters, 202,108-3.

Khataee, A., Saadi, S., Safarpour, M., Joo, S.W. (2015). Sonocatalytic Performance of Er-Doped Zno for Degradation of a Textile Dye. Ultrasonics Sonochemistry 27, 379–88.

Hyunghoon, K., Moon, J.Y., Lee, H.S. (2012). Effect of Zncl2 Concentration on the Growth of Zno by Electrochemical Deposition. Current Applied Physics, 12, 35-S38.

Kumari, B., Sharma, S., Satsangi, V.R., Dass, S., Shrivastav, R. (2015). Surface Deposition of Ag and Au Nano-Isles on Zno Thin Films Yields Enhanced Photoelectrochemical Splitting of Water. Journal of Applied Electrochemistry, 45(4), 299-312.

Li, H., Zhang, W., Guan, L., Li, F., Yao, M. (2015). Visible Light Active Tio2–Zno Composite Films by Cerium and Fluorine Codoping for Photocatalytic Decontamination. Materials Science in Semiconductor Processing, 40, 310–18.

Li, P., Wei, Z., Wu, T., Peng, Q., Li, Y. (2011). Au-Zno Hybrid Nanopyramids and Their Photocatalytic Properties. Journal of American Chemical Society, 133(15), 5660-5663.

Li, Y., Wang, D., Li, W., He, Y. (2015). Photoelectric Conversion Properties of Electrochemically Codeposited Graphene Oxide–Zno Nanocomposite Films. Journal of Alloys and Compounds, 648, 942-50.

Lu, H., Zhai, X., Liu, W., Zhang, M., Guo, M. (2015). Electrodeposition of Hierarchical Zno Nanorod Arrays on Flexible Stainless Steel Mesh for Dye-Sensitized Solar Cell. Thin Solid Films, 586, 46-53.

Mosquera, E., Rojas-Michea, C., Morel, M., Gracia, F., Fuenzalida, V., Zárate, R.A. (2015). Zinc Oxide Nanoparticles with Incorporated Silver: Structural, Morphological, Optical and Vibrational Properties. Applied Surface Science, 347, 561-68.

Nam, G., Kim, B., Leem, J. (2015), Facile Synthesis and an Effective Doping Method for Zno:In3+ Nanorods with Improved Optical Properties. Journal of Alloys and Compounds, 651, 1-7.

Orhan, N., Baykul, M.C. (2012). Characterization of Size-Controlled Zno Nanorods Produced by Electrochemical Deposition Technique." Solid-State Electronics, 78, 147-50.

Öztürk, S., Kösemen, A., Alpaslan Kösemen, Z., Kılın, N., Öztürk, Z.Z., Penza, M. (2016), Electrochemically Growth of Pd Doped Zno Nanorods on QCM for Room Temperature Voc Sensors. Sensors and Actuators B: Chemical, 222, 280–89.

Patil, S.S., Mali, M.G., Tamboli, M.S., Patil, D.R., Kulkarni, M.V., Yoon, H., Kim, H., et al. (2016). Green Approach for Hierarchical Nanostructured Ag-Zno and Their Photocatalytic Performance under Sunlight. Catalysis Today, 260 126-34.

Pradhan, D., Leung, K.T. (2008). Controlled Growth of Two-Dimensional and One-Dimensional Zno Nanostructures on Indium Tin Oxide Coated Glass by Direct Electrodeposition. Langmuir, 24, 9707-9716.

Rahman, M.Y.A., Roza, L., Umar, A.A., Salleh, M.M. (2015). Effect of Boric Acid Composition on the Properties of Zno Thin Film Nanotubes and the Performance of Dye-Sensitized Solar Cell (Dssc). Journal of Alloys and Compounds, 648, 86-91.

Sahu, R.K., Ganguly, K., Mishra, T., Mishra, M., Ningthoujam, R.S., Roy, S.K., Pathak, L.C. (2012). Stabilization of Intrinsic Defects at High Temperatures in Zno Nanoparticles by Ag Modification. Journal of Colloid and Interface Science, 366(1), 8-15.

Shewale, P.S., Yu. Y.S. (2016). Structural, Surface Morphological and Uv Photodetection Properties of Pulsed Laser Deposited Mg-Doped Zno Nanorods: Effect of Growth Time. Journal of Alloys and Compounds, 654, 79-86.

Skompska, M., Zarebska, K. (2014). Electrodeposition of Zno Nanorod Arrays on Transparent Conducting Substrates–a Review. Electrochimica Acta, 127, 467-488.

Tang, K., Gu, S., Liu, J., Ye, J., Zhu, S., Zheng, Y. (2015). Effects of Indium Doping on the Crystallographic, Morphological, Electrical, and Optical Properties of Highly Crystalline Zno Film. Journal of Alloys and Compounds, 653, 643-648.

Udom, I. , Ram, M.K., Stefanakos, E.K., Hepp, A.F., Goswami, D.Y. (2013). One Dimensional-Zno Nanostructures: Synthesis, Properties and Environmental Applications. Materials Science in Semiconductor Processing, 16, 2070-2083.

Vanalakar, S.A., Patil, V.L., Harale, N.S., Vhanalakar, S.A., Gang, M.G., Kim, J.Y., Patil, P.S., Kim, J.H. (2015). Controlled Growth of Zno Nanorod Arrays Via Wet Chemical Route for No2 Gas Sensor Applications. Sensors and Actuators B: Chemical, 221, 1195–1201.

Wang, R., Su. W. (2016). Valence Control and Periodic Structures in Cu-Doped Zno Nanowires. Journal of Alloys and Compounds, 654, 1-7.

Xu, F., Chen, J., Guo, L., Lei, S., Ni. Y. (2012). In Situ Electrochemically Etching-Derived Zno Nanotube Arrays for Highly Efficient and Facilely Recyclable Photocatalyst. Applied Surface Science 258, 8160–8165.

Yoo, R., Cho, S., Song, M., Leea, W. (2015). Highly Sensitive Gas Sensor Based on Al-Doped Zno Nanoparticles for Detection of Dimethyl Methylphosphonate as a Chemical Warfare Agent Simulant. Sensors and Actuators B: Chemical, 221, 217–223.

Zhang, Y., Ram, M.K., Stefanakos, E.K., Goswami, D.Y. (2012). Synthesis, Characterization, and Applications of Znonanowires. Journal of Nanomaterials 2012, 1-22.

Zulkifli, Z., Kalita, G., Tanemura, M. (2015). Fabrication of Transparent and Flexible Carbon-Doped Zno Field Emission Display on Plastic Substrate. Physica Status Solidi 9,145-148.